FULL PAPER

Fracture of ankle: MRI using opposed-phase imaging obtained from turbo spin echo modified Dixon image shows improved sensitivity

[1]JIN HEE YOU, MD, [1,2]IN HWAN KIM, MD, [3]JINWOO HWANG, MS, [4]HYE SUN LEE, PhD and [1]EUN HAE PARK, MD

[1]Department of Radiology, Research Institute of Clinical Medicine of Chonbuk National University - Biomedical Research Institute of Chonbuk National University Hospital, Chonbuk National University Medical School, Jeonju, South Korea
[2]Department of Radiology, Jeonju Wooridul Spine Hospital, Jeonju, Republic of Korea
[3]Clinical Science, Philips Healthcare, Seoul, Republic of Korea
[4]Biostatistics Collaboration Unit, Yonsei University College of Medicine, Seoul, South Korea

Address correspondence to: Prof Eun Hae Park
E-mail: *mbgracie@gmail.com*

Objective: To evaluate if opposed-phase (OP) imaging obtained from the turbo spin echo (TSE) modified Dixon (mDixon) technique can increase the sensitivity of MRI for diagnosing ankle fractures.

Methods: This study included 95 CT-confirmed ankle fractures with additional MRI of the ankle using a TSE modified Dixon (mDixon) technique. Two groups of images were analyzed independently: Group 1—imaging group without OP imaging; Group 2—imaging group with OP imaging. Readers assessed the images using a 4-point confidence score to detect fractures. During the first review session, the fracture site was blinded. For the second review session, the fracture site was provided. Sensitivity and positive-predictive value were calculated.

Results: In both sessions, the sensitivity for Group 2 was significantly greater than that for Group 1 (Session 1: 76.3% *vs* 62.6%, *p* < 0.0001; Session 2: 80.5% *vs* 65.3%, *p* < 0.0001). The positive-predictive value of Group 2 was significantly lower in both sessions 1 and 2 (Session 1: 85.8% *vs* 97.5%, *p* < 0.0001; Session 2: 90.5% *vs* 96.9%,

p = 0.0068). Among the 28 false-negative fractures missed in Group 1 (Session 1), 12 (9 minimal displaced and 4 small diameter fractures) were identified in Group 2 (Session 1). While 8.9% showed lower movement, 33.6% showed upper movement in Group 2 compared with Group 1. Possible causes of false-positive lesions were subcutaneous fat, bone marrow edema, and intra-osseous vessel mimic fractures.

Conclusion: OP imaging obtained using the modified Dixon technique provided better sensitivity and improved descriptions of fractures, especially for minimal displaced fractures and small diameter fractures. However, caution is required when diagnosing fractures with OP imaging because pseudofractures can appear as a result of adjacent bone marrow edema, vascular structures, or subcutaneous fat lobules.

Advances in knowledge: In MRI, minimal displaced or small chip bone fracture maybe missed, OP imaging obtained using the mDixon technique provided better sensitivity and improved descriptions of fractures using the black boundary artifact.

INTRODUCTION

The ankle is the second most commonly injured body site in sports, after the knee. The most common type of ankle injury is an ankle ligamentous sprain. Since MRI provides excellent evaluation of ankle ligaments, MRI is frequently performed for ankle injuries. However, MRI may show unsatisfactory results regarding certain types of fractures, including small cortical fractures and minimal displaced fractures compared with CT.[1–3] Since not all patients with ankle injury undergo both CT and MRI, such fractures can be missed in patients who only undergo MRI.

Recently, the Dixon technique has been applied in MRI of distal extremities, including the ankle.[4,5] The Dixon method for fat suppression was described by Dixon in 1984, and is based on the chemical shift phenomenon.[6] This technique has gained attention because it can achieve uniform fat suppression. Without additional scans, one acquisition of a Dixon image automatically reconstructs to four different images using a fat–water separation algorithm: water-only, fat-only, in-phase (IP), and opposed-phase (OP) imaging.[7] Among these, OP imaging shows a characteristic artifact called the black boundary artifact or India ink artifact; thick dark lines are seen at the boundaries of different kinds of

Figure 1. (A, B) Axial T_1 chemical shift IP (A) and OP imaging (B). Note that the organ margins are outlined with a thick dark signal line (arrows) in OP imaging (B), an artifact referred to as the India ink artifact. (C–E), Sagittal T_2 mDixon IP (C), OP imaging (D) of ankle, and corresponding ankle CT (E). Fracture in (E) (arrow) is well depicted in both (C, D) (arrows in C, D). Note that the contrast of the fracture line is better for (D) with an India ink artifact (white arrow). IP, in-phase; mDixon, modified Dixon; OP, opposed-phase.
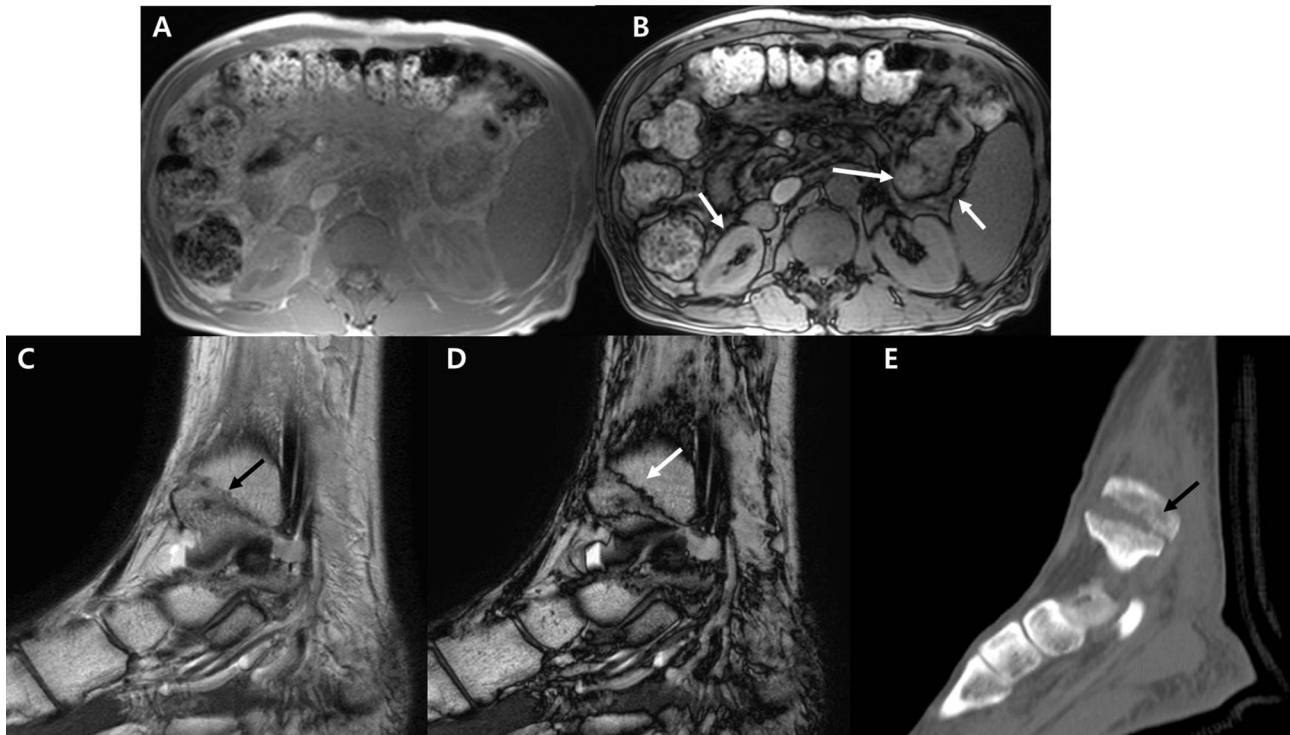
soft tissues.[8,9] In abdominal imaging, the margins of organs are outlined with a dark signal band (Figure 1a,b). Similarly, a dark signal line from an India ink artifact can be observed at a fracture line in OP imaging due to the composition of water and fat from bone marrow along that line (Figure 1c–e).[10,11] In cases where MRI is required for assessing ankle injury, OP imaging from mDixon MRI may allow improved fracture detection without any diagnostic loss compared to conventional MRI. However, to the best of our knowledge, there are no reports on using Dixon OP MRI to assess ankle injuries. Therefore, the objective of this study was to evaluate if OP imaging obtained from the turbo spin echo (TSE) mDixon technique can increase the sensitivity of MRI for diagnosing ankle fractures compared with conventional MRI techniques.

METHODS AND MATERIALS
This retrospective study was approved by our Institutional Review Board for Human Research. The requirement for informed consent was waived.

Subjects
From March 2015 to June 2015, a total of 148 consecutive patients with ankle discomfort underwent ankle MRI from our emergency trauma center or orthopedic department. Among them, 59 patients underwent lower extremity or ankle CT within the previous or subsequent week, and the imaging reports in the institutional medical database were reviewed retrospectively for the keyword "fracture." All patients were examined by an orthopedic

surgeon. Inclusion criteria included: (1) patients older than 18 years, and (2) patients who had clinical and radiologic diagnosis of fracture. Exclusion criteria were as follows: (1) MRI performed without the Dixon technique ($n = 4$), (2) MRI without OP imaging ($n = 3$), (3) patients with susceptibility artifacts from metal or air near the trauma site ($n = 3$), (4) remote fractures ($n = 4$), (5) insufficiency fracture ($n = 0$), (6) impaction fracture ($n = 0$), and (7) incomplete fracture ($n = 0$). A total of 45 patients (34 males and 11 females; age range, 18–82 years) with 95 fractures fit the inclusion criteria. The fracture numbers were distributed as follows: patients with one fracture ($n = 20$), two fractures ($n = 13$), three fractures ($n = 4$), four fractures ($n = 5$), and five or more fractures ($n = 3$).

Imaging acquisition
All MRI examinations were performed using a 3.0 T MRI system [Achieva 3T TX, Philips Healthcare with a two-point modified Dixon (mDixon) technique or Skyra, Siemens Healthcare, Erlangen, Germany with a three-point mDixon technique] with an eight-element phased-array ankle coil using the TSE mDixon technique. Conventional T_1 weighted axial TSE was performed first, followed by TSE T_2 weighted mDixon in axial, coronal, and sagittal planes. For patients suspicious for inflammation, infection, or mass, post-contrast images were obtained by TSE T_1 weighted Dixon in axial, coronal, and sagittal planes (Table 1) using gadoterate meglumine (Dotarem®, Guerbet, France). From a single acquisition using the Dixon technique, images were reconstructed into four different images by a fat–water separation algorithm: water-only, fat-only, IP, and OP imaging.[7,12]

Table 1. Parameters of MRI

	Axial *T*1 weighted	Axial *T*2 weighted mDixon	Coronal *T*2 weighted mDixon	Sagittal *T*2 weighted mDixon
TR (ms)	620	4100	2000	5000
TE (ms)	11	59	60	58
NEX	1	1	1	1
FOV (mm)	139–180	150×150	150×150	160×160
Matrix	512×317	448×269	448×282	448×314
Voxel size (mm)	$0.3 \times 0.3 \times 2.5$	$0.3 \times 0.3 \times 2.5$	$0.3 \times 0.3 \times 3.0$	$0.4 \times 0.4 \times 3.0$
Slice thickness (mm)	2.5	2.5	3	3
Slice gap (mm)	0.25	0.25	0.3	0.6
Bandwidth (Hz/pixel)	257	207	260	211
Imaging time (min:s)	2:12	3:25	3:04	2:25

FOV, field of view; NEX, number of excitations; mDixon, modified Dixon; TE, echo time; TR, repetition time.

Ankle CT scans were performed using a Brilliance iCT scanner (Philips Healthcare, Cleveland, OH) with 120 kVp, 150 mm field of view, and 0.5 mm slice thickness. The scanner was calibrated daily. CT scans were performed with patients in the supine position. Multidetector CT and three-dimensional reconstructions were performed.

Radiographic images were retrieved using Picture Archiving and Communication System, and measurements were subsequently carried out using Picture Archiving and Communication System software (IMPAX; Agfa Healthcare, Mortsel, Belgium).

Image analysis

Two experienced musculoskeletal radiologists retrospectively and independently evaluated all images to detect fractures. Reader 1 had 5 years of experience in musculoskeletal radiology, and Reader 2 had 9 years of experience in musculoskeletal radiology.

The image review consisted of two reviewing sessions for two image groups, with a 2 week interval between each session.

In the first session, radiologists were blinded to imaging reports, clinical history, clinical findings, and fracture site. To prevent recall bias, the order of images was randomized independently, and readers reviewed the MR images in separate groups. Group 1 had imaging without OP imaging, including axial T_1 weighted image (WI), coronal, sagittal, and axial T_2 weighted mDixon water phase (considered to be conventional fat-suppressed T_2WI), and IP images (considered to be conventional T_2WI). Group 2 was the OP imaging group and contained coronal, sagittal, and T_2 mDixon OP.

In the second session, readers once again reviewed the two groups of MR images, but the site of the fracture was provided. In addition, readers also speculated on possible causes of false-positive or false-negative results.

In both sessions, the readers assigned a confidence level to each fracture diagnosis using a 4-point scale: (0) no fracture; (1) questionable; (2) definite fracture; (3) definite fracture with possible description. MR images in which lesions were not detected were given a rating of 0.

Fractures were defined when either a cortical disruption or linear abnormal low signal intensity was shown extending from the trabecular bone to the cortical bone.[13–15]

Reference standard

The reference standard for fracture diagnosis was based on CT. Fractures were diagnosed when either a cortical disruption or linear abnormal density extending from trabecular bone to cortical bone was observed on CT images. The mean interval between MR and CT was 0.92 days (range, 0–3 days).

Statistical analysis

The sensitivity and positive-predictive value (PPV) for each group of images in two sessions were evaluated according to the number of fractures with diagnoses assigned a confidence score of 2 or 3 using generalized estimating equations. Values for the two image groups were then compared using the McNemar test. The lower movement rate and upper movement rate of confidence levels were evaluated based on the McNemar test. *p*-values less than 0.05 and empirical 95% confidence intervals not including 0 indicated statistical significance. All statistical analyses were performed using statistical software (SAS, v. 9.2, SAS Institute, Cary, NC).

RESULTS

Two radiologists confirmed all 95 fractures from lower extremity or ankle CT (all unilateral side) obtained from 45 patients. The most common fracture site was the tibia, including the medial malleolus (22 fractures, 23.2%). The next most common site was the fibula (18 fractures, 18.9%). 12 fractures were at the calcaneus, 8 fractures were at the talus, and 7 fractures were at the second metatarsal bone base. Four fractures were at the fourth

Table 2. Sensitivity for the detection of 95 fractures

		Reader 1		Reader 2		Pooled data	
		Sensitivity	*p*-value	Sensitivity	*p*-value	Sensitivity	*p*-value
Session 1	Group 1	62.1	0.005	63.2	0.0002	62.6	<.0001
	Group 2	74.7		77.9		76.3	
Session 2	Group 1	64.2	<0.0005	66.3	0.005	65.3	<.0001
	Group 2	81.1		80.0		80.5	

metatarsal bone base, and three fractures each were at the cuboid, first metatarsal bone base, and fifth metatarsal bone base. Two fractures each were observed at the navicular, lateral cuneiform, third metatarsal bone base, fourth metatarsal bone head, and first proximal phalanx. Only one fracture each was found at the medial cuneiform; heads of the second, third, and fifth metatarsal bones; and first distal phalanx.

Session 1
For all readers, inspection of Group 2 images yielded significantly higher mean sensitivity than inspection of Group 1 images (76.3% *vs* 62.6%, $p < 0.0001$). The sensitivity of Reader 1 for Group 1 and Group 2 was 62.1 and 74.7%, respectively ($p = 0.005$). The sensitivity of Reader 2 for Group 1 and Group 2 images was 63.2 and 77.9% ($p = 0.0002$), respectively (Table 2). For both readers, the PPV was significantly higher for Group 1 than Group 2 (97.5% *vs* 85.8%, respectively; $p < 0.0001$). The PPV of Reader 1 for Group 1 and Group 2 was 96.7 and 83.5%, respectively ($p = 0.0004$). The PPV of Reader 2 for Group 1 and Group 2 was 98.4 and 88.1% ($p = 0.002$), respectively (Table 3).

In Group 1, there were 28 false-negative fractures missed by both readers 1 and 2. These fractures were located at the second metatarsal base ($n = 5$), tibia ($n = 3$), talus ($n = 3$), fibula ($n = 2$), cuboid ($n = 2$), first metatarsal bone base ($n = 2$), fourth metatarsal bone base ($n = 2$), fifth metatarsal bone base ($n = 2$), first proximal phalanx ($n = 2$), medial malleolus, calcaneus, lateral cuneiform, third metatarsal base, and fourth metatarsal head. Among these 28 false-negative fractures, 22 (78.5%) had minimal displacement, and 14 (50%) were small chip bone fractures. 12 of 28 fractures (42.8%) missed in Group 1 were identified in Group 2 (scored 3 or 4). These fractures were located in the tibia ($n = 2$), first metatarsal base ($n = 2$), second metatarsal base ($n = 2$), medial malleolus, fibula, calcaneus, third and fourth metatarsal base, and first proximal phalanx. 9 of 12 fractures

were minimally-displaced fractures (75%) (Figure 2), and 4 of 12 (33.3%) fractures were small chip bone fractures (Figure 3).

For Group 2 evaluated in Session 1, 23 false-negative fractures were missed by either Reader 1 or Reader 2. Fractures were located at the second metatarsal base ($n = 4$), tibia ($n = 3$), cuboid ($n = 3$), first metatarsal base ($n = 3$), fifth metatarsal bone base ($n = 3$), fourth metatarsal bone base ($n = 2$), fibula, talus, lateral cuneiform, and fourth and fifth metatarsal heads. 17 of 23 fractures (73.9%) had a minimal displaced fragment, and 13 of 23 (56.5%) fractures had a diameter less than 5 mm.

When comparing confidence scores, 8.9% of cases showed lower movement of the confidence score, while 33.6% of cases showed upper movement of the confidence score in Group 2 compared to Group 1 (Figure 4).

The number and site of false-positive fractures noted by either Reader 1 or Reader 2 in each were as follows: Group 1 = 1 (third metatarsal bone base), Group 2 = 8 (third metatarsal base ($n = 3$), navicular bone, cuboid, second and fourth metatarsal bases, fourth metatarsal head).
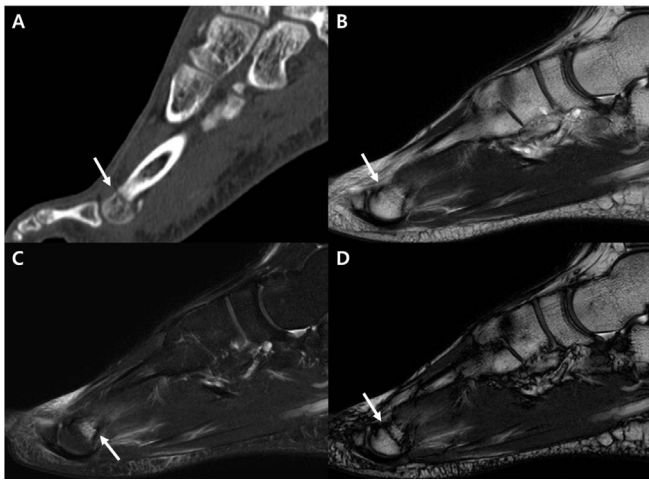
Session 2
The sensitivity of both readers for Group 2 images was higher than for Group 1 images (80.5% *vs* 65.3%, respectively; $p < 0.0001$). The sensitivity of Reader 1 for Group 1 *vs* Group 2 images was 64.2% *vs* 81.1%, respectively ($p = 0.0005$). The sensitivity of Reader 2 for Group 1 versus Group 2 was 66.3% *vs* 80.0%, respectively ($p = 0.004$) (Table 2). For both readers, PPV was significantly higher for Group 1 than Group 2 (96.9% *vs* 90.5%, respectively; $p = 0.0068$). The PPV of Reader 1 for Group 1 *vs* Group 2 was 96.8% *vs* 90.5%, respectively ($p = 0.060$). The PPV of Reader 2 for Group 1 *vs* Group 2 was 96.9% *vs* 90.4%, respectively ($p = 0.052$). While the PPV of Session 2 increased compared to

Table 3. PPVs for the detection of 95 fractures

		Reader 1		Reader 2		Pooled data	
		PPV	*p*-value	PPV	*p*-value	PPV	*p*-value
Session 1	Group 1	96.7	0.0004	98.4	0.002	97.5	<0.0001
	Group 2	83.5		88.1		85.8	
Session 2	Group 1	96.8	0.060	96.9	0.052	96.9	0.006
	Group 2	90.6		90.5		90.5	

PPV, positive-predictive value.

Figure 2. A 19-year-old male with fracture of the fourth metatarsal neck. (A–D), In sagittal ankle CT, (A) the fourth metatarsal neck fracture with minimal displacement is well depicted (arrow). Sagittal IP image obtained using the T_2 weighted mDixon technique (B) shows an subtle linear low signal without definitive cortical staff-off (arrow), which was not interpreted as fracture. Sagittal water-only sequence from T_2 weighted mDixon imaging (C) shows focal bone marrow edema of the fourth metatarsal bone (arrow), which was interpreted as bone marrow contusion. Sagittal OP imaging from T_2 weighted mDixon imaging (D) demonstrates a clear-cut low signal line crossing the neck of the fourth metatarsal bone resulting from India ink artifact (arrow); this was considered to be the fracture line. IP, in-phase; mDixon, modified Dixon; OP, opposed-phase.

Figure 3. A 65-year-old female with tibial posterior lip chip fracture. (A–D) The sagittal ankle CT image (A) depicts the posterior lip of the tibia chip fracture with minimal displacement (arrows). Sagittal IP imaging from T_2 weighted mDixon technique (B) shows no definitive fracture line (circle). The low signal structure inferior to the cortex is the transverse posterior ligament (arrowheads). Sagittal water-only sequence from the T_2 weighted mDixon imaging (C) shows bone marrow edema (arrow) at the posterior lip of the tibia, which we interpreted as bone marrow contusion. Sagittal OP imaging from T_2 weighted mDixon imaging (D) demonstrates a clear-cut low signal line resulting from an India ink artifact (arrow) corresponding to the fracture line. IP, in-phase; mDixon, modified Dixon; OP, opposed-phase.

that of Session 1 for Group 2 (90.5% *vs* 85.8%, respectively), the PPV decreased at Session 2 compared with Session 1 for Group 1 (96.9% *vs* 97.5%, respectively) (Table 3).
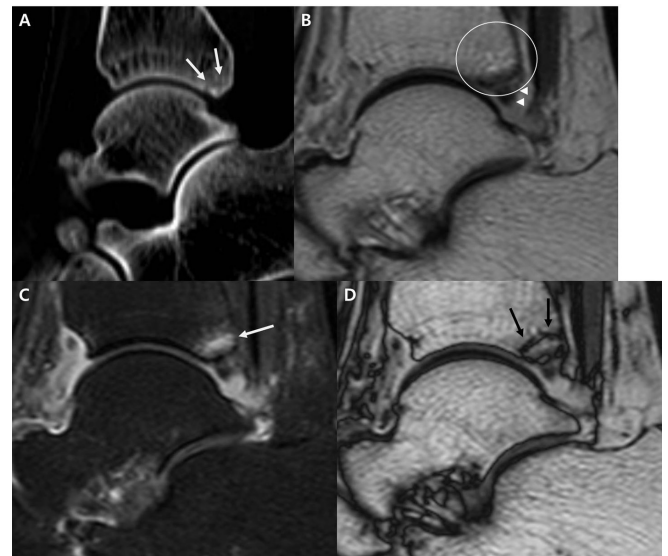
In Group 1, there were 19 false-negative fractures missed by both readers 1 and 2. Among these 19 false-negative fractures, 16 (84.2%) had minimal displacement, and 8 (42.1%) were small chip bone fractures. 14 of 19 fractures (73.6%) missed in Group 1 were identified in Group 2 (scored 3 or 4). 12 of 14 fractures were minimal displaced fractures (85.7%), and 7 of 14 (50%) fractures were small chip bone fractures (Figure 5).

In Group 2 evaluated during Session 2, 8 among 23 false-negative fractures missed in Session 1 were still not verified. These fractures were located at the second metatarsal base ($n = 3$), tibia, lateral cuneiform, cuboid, and fourth and fifth metatarsal bases. Five of eight fractures (62.5%) had a minimal displaced fragment, and six of eight fractures (75%) had a diameter less than 5 mm (Figure 6).

When comparing confidence scores, 8.9% of cases showed lower movement of confidence score, while 39.4% of cases showed upper movement of confidence score in group2 compared to group1(Figure 4).

The number and site of false-positive fractures noted by either Reader 1 or Reader 2 in each group were as follows: Group 1

= 4 [fibula ($n = 3$), third metatarsal base], Group 2 = 17 [third metatarsal base ($n = 3$); talus ($n = 2$); tibia; fibula; navicular bone; medial cuneiform; cuboid; intermediate cuneiform; first, second, and fourth metatarsal bases; and first, fourth, and fifth metatarsal heads]. Pseudolesions, such as subcutaneous fat lobules, bone marrow edema from contusions, or vascular structures, were misinterpreted as fractures in Group 2 images.

DISCUSSION

Dixon imaging has been difficult to implement in clinical practice until recently, especially in joint imaging, which involves greater magnetic field inhomogeneity than other anatomical sites. The original Dixon method provides water-only and fat-only images from a simple spectroscopic imaging technique, but it is sensitive to magnetic field inhomogeneity, which results in incomplete water and fat separation. Substantial improvement and technical advances have been made in the past few decades. Effective phase correction techniques, including a phase unwrapping algorithm, remove B0 field inhomogeneity so that water–fat separation is reliably achieved.[16–20] Data acquisition techniques and advanced performance of modern MR hardware minimize scan time and increase the signal-to-noise ratio.[21] As a result of these improvements, major MR vendors are now providing commercially available, fast, and reliable Dixon techniques for joint imaging.

Figure 4. Graph shows the number and percentage of confidence scores for groups 1 and 2 from sessions 1 and 2.
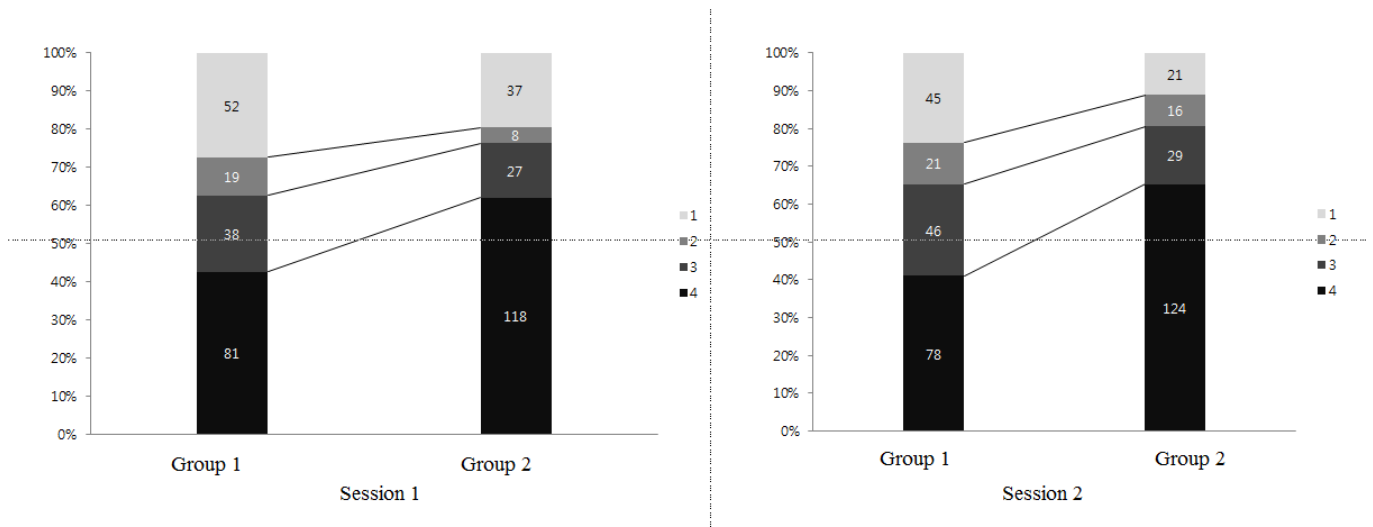
Over the past few years, the number of studies using Dixon techniques for bone and joints has increased.[4,5,10,22–30]

Our study results demonstrate that the sensitivities for the image group that contained OP imaging (Group 2) were significantly higher than those for the image group that did not contain OP imaging (Group 1). The overall sensitivity for fractures in Group 1 was in general accordance with previous data. Mallee et al[31] reported that MRI had a sensitivity of 67% for detecting scaphoid fractures. However, the sensitivity of MRI for detecting fractures varies from 33.3 to 100%.[2,13–15,31–33] This wide range of sensitivities might be related to differences in the mechanism, location, orientation, and type of fracture, as well as the MRI protocol used. The low diagnostic performance of MRI for certain types of fracture, including cortical fractures, minimal displaced fractures, avulsion fracture, and distraction fracture, is well-known.[2,10,14,33]

The higher sensitivity attained in Group 2 might be due to the artifact referred to as the black boundary artifact or India ink artifact that is associated with OP imaging. These artifacts, which

are dark lines at the interfaces between fat and water, are due to chemical shift imaging (Figure 1b,d). Voxels at the interfaces between tissues are composed of both fat and water. In such voxels of OP imaging, signals from each tissue are canceled, resulting in the characteristic dark ink-like line of the object. This artifact is useful for identifying fat within a mainly water-containing structure.[8,9] The fracture line is technically where water is located within mainly fat-containing bone marrow; hence, the resulting thick linear dark signal in fracture line provides better contrast and increases sensitivity for detecting fractures. The fracture line maybe stressed better also in fat-only imaging. Wohlgemuth et al[11] introduced a case showing that fat-only imaging better depicted the fracture line compared with water-only imaging or Short tau inversion recovery. They explained this as a result of bone marrow edema, and the fracture line was hypointense in a high-signal background for bone marrow in the fat-only sequence. However, to the best of our knowledge, the comparison for detecting fractures between OP imaging and fat-only imaging has not been evaluated and further research is required.

Figure 5. A 31-year-old male with fracture of the anterior aspect of the medial malleolus. (A–C) Axial ankle CT (A) shows medial malleolar fracture with a small fracture fragment (arrow). In axial IP imaging using the T_2 weighted mDixon technique (B), the fracture fragment is very vague, and the fracture was missed by both readers in sessions 1 and 2. Axial OP imaging from T_2 weighted mDixon technique (C) demonstrates a small fracture fragment outlined with a dark signal line from an India ink artifact (arrow). IP, in-phase; mDixon, modified Dixon; OP, opposed-phase.
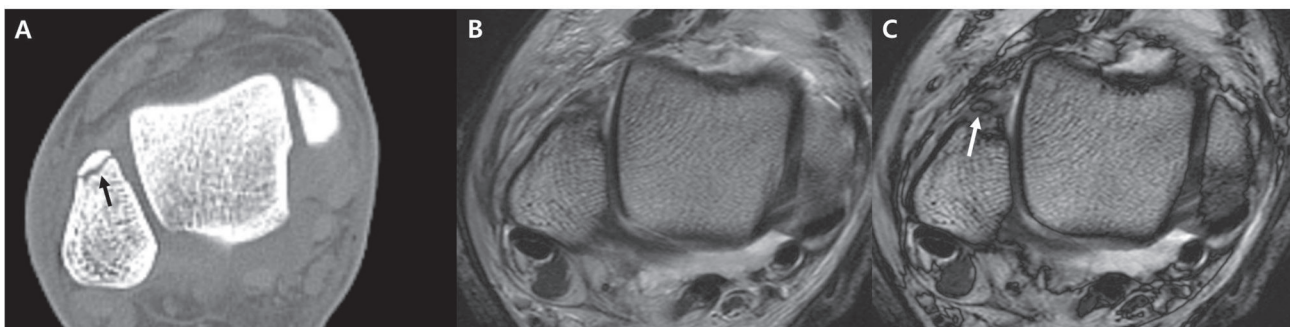
Figure 6. A 53 year-old male with a lateral cuneiform cortical fracture. Axial ankle CT (A) shows two small fracture fragments located lateral to the lateral cuneiform (arrows). (B–E) The fracture fragment was not detected by either reader in either Session 1 or Session 2 in the axial T_1 weighted (B), IP imaging (C), water-only imaging (D), and OP imaging (E) from the T_2 weighted mDixon technique. Note that the fracture fragment is small with low signal intensity (arrows in B–E); this could be interpreted as a ligamentous structure. IP, in-phase; mDixon, modified Dixon; OP, opposed-phase.
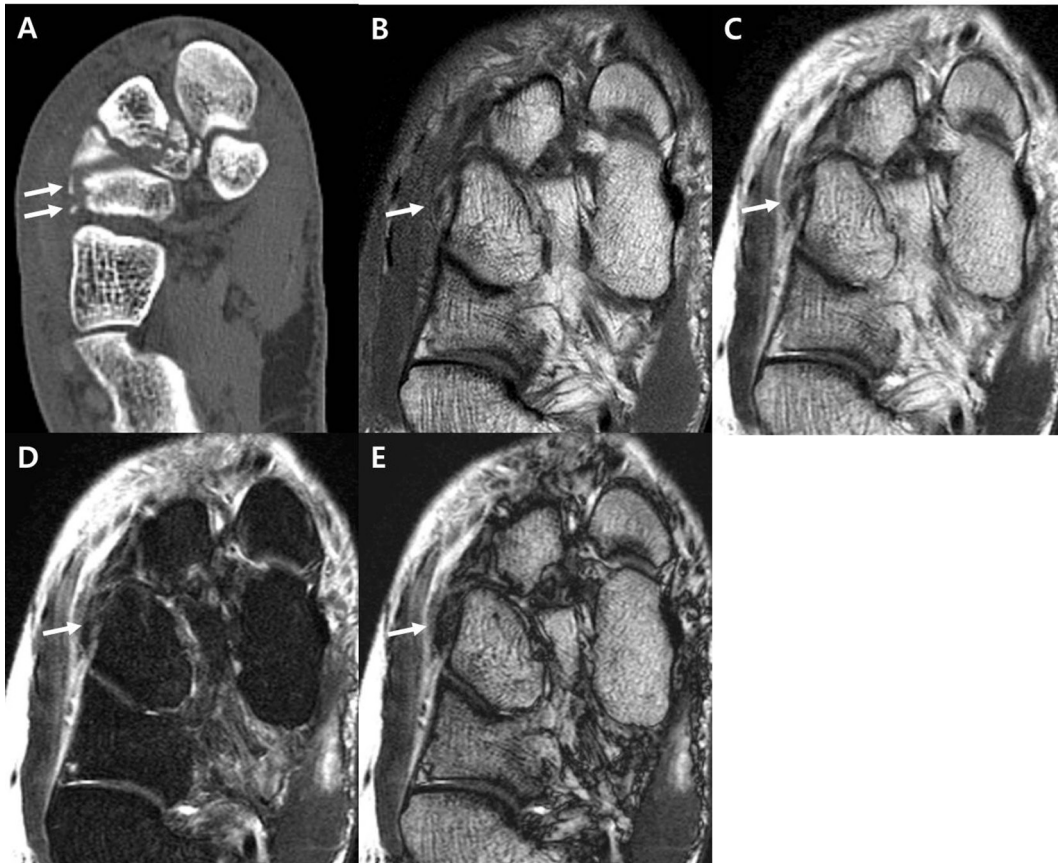
A considerable number of false-negative fractures missed in Group 1 were discerned in Group 2 (Figure 6). In Session 1, 12 of 28 false-negative fractures missed by both readers in Group 1 were identified in Group 2. In Session 2, 14 of 19 false-negative fractures in Group 1 missed by both readers were identified. One notable finding of this study is that a considerable number of minimally-displaced fracture missed in Group 1 were identified in Group 2 (Figure 2): 9 of 22 (40%) in Session 1 and 12 of 16 (75%) in Session 2. In a minimal displaced fracture, bone marrow edema maybe the only finding of MRI without a definitive cortical staff-off. Such case is challenging to differentiate from a bone marrow contusion. According to Palmer et al[14] cases of a minimally-displaced fracture without adjacent BM edema can be difficult to detect. MRI provides inadequate depiction of small avulsion fractures or chip fractures. Because of the low signal intensity of the cortex, thin cortical avulsion can be interpreted as ligament avulsion.[2] In an MRI study of 12 patients with Segond fractures, the fractures were only visible one-third of the time because edema and hemorrhage in the surrounding soft tissue obscured the small fracture.[33] Our results of fractures with a diameter less than 5 mm in Group 1 were in general accordance with previously-mentioned studies. However, in Group 2, some fractures with a diameter less than 5 mm not depicted in Group

1 could be identified; 4 out of 14 (28.5%) in Session 1 and 7 out of 8 (87.5%) in Session 2.

We found upper movement of the confidence score based on inspection of Group 2 *vs* Group 1 images. Being able to describe a fracture is an integral part of deciding fracture treatment. The type of fracture treatment is closely associated with age, mode of trauma, location, type of fracture, degree of displacement, direction of displacement, alignment, and articular extension. The dark line/black boundary artifact seen in Group 2 enabled better description and description of fracture status.

Even when the fracture site was specified (Session 2), MRI was not very sensitive for detecting fractures. These results might be explained by the strict inclusion criteria of this study, as we minimally included any fractures known to have unsatisfactory outcomes of detection by CT. Certain types of fracture, including insufficiency fracture, stress fracture, and impacted fracture, are known to show a lower diagnostic performance in radiograph or CT.[2,14,34] Cabarrus et al[34] compared the images of CT and MRI in detecting 129 insufficiency fractures of pelvis and femur, with a sensitivity significantly higher on MRI than on CT (99% *vs* 69%, respectively). Though small avulsion fractures were better

discerned using Group 2 images than Group 1 images, there were still three avulsion fractures missed by each reader during Session 2. Another possible reason for the unsatisfactory sensitivity of MRI is that a considerable number of fractures were interpreted as bone marrow edema, vessels, or subcutaneous fat lobules. Black boundary artifacts result in a dark signal line to the fascia. Superficial fascia is known to have three layers: membranous layer, retinacula cutis superficialis, and retinacula cutis profundus. Because of the retinacular pattern of the superficial fascia, subcutaneous fat and the surrounding fascia can mimic a fracture. When a fracture is being evaluated, one should kept these pitfalls in mind.

While the PPV of Group 2 increased in Session 2 compared with Session 1, the PPV of Group 1 decreased in Session 2 compared with Session 1. During Session 2, only the name of the fractured bone was provided, which might have caused readers to assess uncertain or questionable lesions as definitive fractures.

Our study had several limitations. First, the MR images were analyzed retrospectively. However, consecutive patients who satisfied the inclusion criteria were recruited to minimize the possibility of selection bias. Second, this study included only patients diagnosed with fracture on the basis of multidetector CT. This might have introduced selection bias and reader bias. To minimize selection bias, we excluded certain types of fracture known to show unsatisfactory diagnostic performance in CT fracture detection. To minimize reader bias, readers were blinded to the exact site as well as number of fractures in the first session. For this reason, we were unable to calculate specificity or negative-predictive value. Fourth, the possible causes of false-positive or false-negative fractures were not statistically evaluated. Possible causes include adjacent subcutaneous fat lobules, bone marrow edema, and vascular structures. Further evaluation focusing on the reasons for false-positive or false-negative fractures is needed to improve the accuracy of MRI or the Dixon technique for diagnosing fractures. Fifth, the possibility of recall bias should be considered. However, this was avoided by interval review with an at least 2-week interval and by randomizing the order in which cases were reviewed. Sixth, for the conventional MRI group (Group 1), we did not perform conventional TSE T_2WI or TSE fat-suppressed T_2WI. In this study, Group 1 comprised conventional MR images. Because the Dixon technique can provide both T_2WI and T_2WI with fat suppression from a single acquisition, mDixon water-only image was considered to be equivalent to conventional fat-suppressed T_2WI, and IP imaging was considered to be conventional T_2WI. The middle echo from the source image obtained using the Dixon technique with 0° phase offset is a T_2WI, and because the Dixon technique acquires multiple echoes within a single pass, fat-suppressed T_2WI can be obtained.[11,29,35,36] Finally, the fractures evaluated in this study were limited to the ankle. Since MRI is usually performed for all joint injuries, we expect OP imaging to give similar outcomes to other joints evaluated with mDixon MRI, although further study is warranted.

CONCLUSIONS
OP imaging obtained using the mDixon technique provided better sensitivity and improved fracture description than conventional MRI, especially for minimally-displaced fractures and small chip bone fractures.

However, caution is required when diagnosing fractures with OP imaging because pseudofractures can appear as a result of adjacent bone marrow edema, vascular structures, or subcutaneous fat lobules.

REFERENCES

1. Perrich KD, Goodwin DW, Hecht PJ, Cheung Y. Ankle ligaments on MRI: appearance of normal and injured ligaments. *AJR Am J Roentgenol* 2009; **193**: 687–95. doi: https://doi.org/10.2214/AJR.08.2286

2. Lohman M, Kivisaari A, Kallio P, Puntila J, Vehmas T, Kivisaari L. Acute paediatric ankle trauma: MRI versus plain radiography. *Skeletal Radiol* 2001; **30**: 504–11. doi: https://doi.org/10.1007/s002560100376

3. Hølmer P, Søndergaard L, Konradsen L, Nielsen PT, Jørgensen LN. Epidemiology of sprains in the lateral ankle and foot. *Foot Ankle Int* 1994; **15**: 72–4. doi: https://doi.org/10.1177/107110079401500204

4. Maas M, Dijkstra PF, Akkerman EM. Uniform fat suppression in hands and feet through the use of two-point dixon chemical shift MR imaging. *Radiology* 1999; **210**: 189–93. doi: https://doi.org/10.1148/radiology.210.1.r99ja35189

5. Nozaki T, Tasaki A, Horiuchi S, Osakabe C, Ohde S, Saida Y, et al. Quantification of fatty degeneration within the supraspinatus muscle by using a 2-point dixon method on 3-T MRI. *AJR Am J Roentgenol* 2015; **205**: 116–22. doi: https://doi.org/10.2214/AJR.14.13518

6. Dixon WT. Simple proton spectroscopic imaging. *Radiology* 1984; **153**: 189–94. doi: https://doi.org/10.1148/radiology.153.1.6089263

7. Eggers H, Brendel B, Duijndam A, Herigault G. Dual-echo dixon imaging with flexible choice of echo times. *Magn Reson Med* 2011; **65**: 96–107. doi: https://doi.org/10.1002/mrm.22578

8. Bley TA, Wieben O, François CJ, Brittain JH, Reeder SB. Fat and water magnetic resonance imaging. *J Magn Reson Imaging* 2010; **31**: 4–18. doi: https://doi.org/10.1002/jmri.21895

9. Pokharel SS, Macura KJ, Kamel IR, Zaheer A. Current MR imaging lipid detection techniques for diagnosis of lesions in the abdomen and pelvis. *Radiographics* 2013; **33**: 681–702. doi: https://doi.org/10.1148/rg.333125068

10. Park EH, Lee KB. Usefulness of black boundary artifact on opposed-phase imaging from turbo spin-echo two-point mDixon MRI for delineation of an arthroscopically confirmed small fracture of the lateral talar dome: a case report. *Medicine* 2017; **96**: e9497. doi: https://doi.org/10.1097/MD.0000000000009497

11. Wohlgemuth WA, Roemer FW, Bohndorf K. Short tau inversion recovery and three-point Dixon water-fat separation sequences in acute traumatic bone fractures at open 0.35 tesla MRI. *Skeletal Radiol* 2002; **31**: 343–8. doi: https://doi.org/10.1007/s00256-002-0517-9

12. Ma J. Dixon techniques for water and fat imaging. *J Magn Reson Imaging* 2008; **28**: 543–58. doi: https://doi.org/10.1002/jmri.21492

13. Deutsch AL, Mink JH, Waxman AD. Occult fractures of the proximal femur: MR imaging. *Radiology* 1989; **170**: 113–6. doi: https://doi.org/10.1148/radiology.170.1.2909083

14. Palmer WE, Levine SM, Dupuy DE. Knee and shoulder fractures: association of fracture detection and marrow edema on MR images with mechanism of injury. *Radiology* 1997; **204**: 395–401. doi: https://doi.org/10.1148/radiology.204.2.9240526

15. Stallenberg B, Gevenois PA, Sintzoff SA, Matos C, Andrianne Y, Struyven J. Fracture of the posterior aspect of the lateral tibial plateau: radiographic sign of anterior cruciate ligament tear. *Radiology* 1993; **187**: 821–5. doi: https://doi.org/10.1148/radiology.187.3.8497638

16. Yeung HN, Kormos DW. Separation of true fat and water images by correcting magnetic field inhomogeneity in situ. *Radiology* 1986; **159**: 783–6. doi: https://doi.org/10.1148/radiology.159.3.3704157

17. Glover GH, Schneider E. Three-point Dixon technique for true water/fat decomposition with B0 inhomogeneity correction. *Magn Reson Med* 1991; **18**: 371–83. doi: https://doi.org/10.1002/mrm.1910180211

18. Low RN, Ma J, Panchal N. Fast spin-echo triple-echo Dixon: initial clinical experience with a novel pulse sequence for fat-suppressed T2-weighted abdominal MR imaging. *J Magn Reson Imaging* 2009; **30**: 569–77. doi: https://doi.org/10.1002/jmri.21880

19. Ma J, Singh SK, Kumar AJ, Leeds NE, Zhan J. T2-weighted spine imaging with a fast three-point dixon technique: comparison with chemical shift selective fat suppression. *J Magn Reson Imaging* 2004; **20**: 1025–9. doi: https://doi.org/10.1002/jmri.20201

20. Ma J, Singh SK, Kumar AJ, Leeds NE, Broemeling LD. Method for efficient fast spin echo Dixon imaging. *Magn Reson Med* 2002; **48**: 1021–7. doi: https://doi.org/10.1002/mrm.10306

21. Ma J, Jackson EF, Kumar AJ, Ginsberg LE. Improving fat-suppressed T2-weighted imaging of the head and neck with 2 fast spin-echo dixon techniques: initial experiences. *AJNR Am J Neuroradiol* 2009; **30**: 42–5. doi: https://doi.org/10.3174/ajnr.A1132

22. Bredella MA, Losasso C, Moelleken SC, Huegli RW, Genant HK, Tirman PF. Three-point Dixon chemical-shift imaging for evaluating articular cartilage defects in the knee joint on a low-field-strength open magnet. *AJR Am J Roentgenol* 2001; **177**: 1371–5. doi: https://doi.org/10.2214/ajr.177.6.1771371

23. Gyftopoulos S, Yemin A, Mulholland T, Bloom M, Storey P, Geppert C, et al. 3DMR osseous reconstructions of the shoulder using a gradient-echo based two-point Dixon reconstruction: a feasibility study. *Skeletal Radiol* 2013; **42**: 347–52. doi: https://doi.org/10.1007/s00256-012-1489-z

24. Hollak C, Maas M, Akkerman E, den Heeten A, Aerts H. Dixon quantitative chemical shift imaging is a sensitive tool for the evaluation of bone marrow responses to individualized doses of enzyme supplementation therapy in type 1 Gaucher disease. *Blood Cells Mol Dis* 2001; **27**: 1005–12. doi: https://doi.org/10.1006/bcmd.2001.0474

25. Kim YP, Kannengiesser S, Paek MY, Kim S, Chung TS, Yoo YH, et al. Differentiation between focal malignant marrow-replacing lesions and benign red marrow deposition of the spine with T2*-corrected fat-signal fraction map using a three-echo volume interpolated breath-hold gradient echo Dixon sequence. *Korean J Radiol* 2014; **15**: 781–91. doi: https://doi.org/10.3348/kjr.2014.15.6.781

26. Lee SH, Lee YH, Hahn S, Suh JS. Fat fraction estimation of morphologically normal lumbar vertebrae using the two-point mDixon turbo spin-echo MRI with flexible echo times and multipeak spectral model of fat: Comparison between cancer and non-cancer patients. *Magn Reson Imaging* 2016; **34**: 1114–20. doi: https://doi.org/10.1016/j.mri.2016.05.007

27. Lee JB, Cha JG, Lee MH, Lee YK, Lee EH, Jeon CH. Usefulness of IDEAL T2-weighted FSE and SPGR imaging in reducing metallic artifacts in the postoperative ankles with metallic hardware. *Skeletal Radiol* 2013; **42**: 239–47. doi: https://doi.org/10.1007/s00256-012-1449-7

28. Hahn S, Lee YH, Suh JS. Detection of vertebral metastases: a comparison between the modified Dixon turbo spin echo T2 weighted MRI and conventional T1 weighted MRI: a preliminary study in a tertiary centre. *Br J Radiol* 2018; **91**: 20170782. doi: https://doi.org/10.1259/bjr.20170782

29. Maeder Y, Dunet V, Richard R, Becce F, Omoumi P. Bone marrow metastases: T2-weighted dixon spin-echo fat images can replace T1-weighted spin-echo images. *Radiology* 2018; **286**: 948–59. doi: https://doi.org/10.1148/radiol.2017170325

30. Douis H, Davies AM, Jeys L, Sian P. Chemical shift MRI can aid in the diagnosis of indeterminate skeletal lesions of the spine. *Eur Radiol* 2016; **26**: 932–40. doi: https://doi.org/10.1007/s00330-015-3898-6

31. Mallee W, Doornberg JN, Ring D, van Dijk CN, Maas M, Goslings JC. Comparison of CT and MRI for diagnosis of suspected scaphoid fractures. *J Bone Joint Surg Am* 2011; **93**: 20–8. doi: https://doi.org/10.2106/JBJS.I.01523

32. Pavić R, Margetić P, Hnatešen D. Diagnosis of occult radial head and neck fracture in adults. *Injury* 2015; **46**(Suppl 6): S119–S124. doi: https://doi.org/10.1016/j.injury.2015.10.050

33. Weber WN, Neumann CH, Barakos JA, Petersen SA, Steinbach LS, Genant HK. Lateral tibial rim (Segond) fractures: MR imaging characteristics. *Radiology* 1991; **180**: 731–4. doi: https://doi.org/10.1148/radiology.180.3.1871286

34. Cabarrus MC, Ambekar A, Lu Y, Link TM. MRI and CT of insufficiency fractures of the pelvis and the proximal femur. *AJR Am J Roentgenol* 2008; **191**: 995–1001. doi: https://doi.org/10.2214/AJR.07.3714

35. Park HJ, Lee SY, Rho MH, Chung EC, Ahn JH, Park JH, et al. Usefulness of the fast spin-echo three-point Dixon (mDixon) image of the knee joint on 3.0-T MRI: comparison with conventional fast spin-echo T2 weighted image. *Br J Radiol* 2016; **89**: 20151074. doi: https://doi.org/10.1259/bjr.20151074

36. Low RN, Austin MJ, Ma J. Fast spin-echo triple echo dixon: Initial clinical experience with a novel pulse sequence for simultaneous fat-suppressed and nonfat-suppressed T2-weighted spine magnetic resonance imaging. *J Magn Reson Imaging* 2011; **33**: 390–400. doi: https://doi.org/10.1002/jmri.22453